Eur. J. Mineral., 34, 549–561, 2022
https://doi.org/10.5194/ejm-34-549-2022
© Author(s) 2022. This work is distributed under
the Creative Commons Attribution 4.0 License.

European Journal of Mineralogy
Open Access

Relatively oxidized conditions for diamond formation at Udachnaya (Siberia)

Luca Faccincani[1], Valerio Cerantola[2,3], Fabrizio Nestola[4], Paolo Nimis[4], Luca Ziberna[5,6], Leonardo Pasqualetto[4], Aleksandr I. Chumakov[3], Jeffrey W. Harris[7], and Massimo Coltorti[1]

[1]Department of Physics and Earth Sciences, University of Ferrara, Via Saragat 1, 44121 Ferrara, Italy
[2]Department of Earth and Environmental Sciences, Università degli Studi di Milano-Bicocca, Piazza della Scienza 4, 20126 Milan, Italy
[3]ESRF – the European Synchrotron Radiation Facility, CS40220, 38043 Grenoble CEDEX 9, France
[4]Department of Geosciences, University of Padua, Via Gradenigo 6, 35131 Padua, Italy
[5]Department of Mathematics and Geoscience, University of Trieste, Via Weiss 2, 34128 Trieste, Italy
[6]Bayerisches Geoinstitut, University of Bayreuth, Universitätsstraße 30, 95440 Bayreuth, Germany
[7]School of Geographical and Earth Sciences, University of Glasgow, Glasgow, G12 8QQ, UK

Correspondence: Luca Faccincani (luca.faccincani@unife.it)

Received: 7 July 2022 – Revised: 22 October 2022 – Accepted: 26 October 2022 – Published: 15 November 2022

Abstract. Thanks to the physical strength of diamonds and their relatively unreactive chemical nature, their mineral inclusions may remain exceptionally preserved from alteration processes and chemical exchanges with surrounding minerals, fluids and/or melts following diamond formation. Cr-bearing spinels are relatively common inclusions found in peridotitic diamonds and important oxybarometers providing information about the oxygen fugacity (fO_2) of their source mantle rocks. Here, we investigated a magnesiochromite–olivine touching pair in a diamond from the Udachnaya kimberlite (Siberia) by in situ single-crystal X-ray diffraction and energy-domain synchrotron Mössbauer spectroscopy, aiming to constrain the physical–chemical conditions of diamond formation and to explore the redox state of this portion of the Siberian craton when the diamond was formed.

The P–T–fO_2 entrapment conditions of the inclusion pair, determined by thermo- and oxybarometric analyses, are $\sim$ 5.7(0.4) GPa and $\sim$ 1015(50) °C (although entrapment at higher T and re-equilibration during subsequent mantle storage are also possible) and fO_2 near the enstatite–magnesite–olivine–diamond (EMOD) buffer. The determined fO_2 is similar to, or slightly more oxidized than, those of xenoliths from Udachnaya, but whilst the xenoliths last equilibrated with the surrounding mantle just prior to their entrainment in the kimberlite at $\sim$ 360 Ma, the last equilibration of the inclusion pair is much older, occurring at 3.5–3.1, $\sim$ 2 or $\sim$ 1.8 Ga before final encapsulation in its host diamond. Hence, the similarity between xenoliths and inclusion fO_2 values indicates that the modern redox state of this portion of the Siberian lithosphere was likely attained relatively early after its formation and may have persisted for billions of years after diamond formation, at least at the local scale. Moreover, the oxygen fugacity determination for the inclusion pair provides direct evidence of diamond formation near the EMOD buffer and is consistent with recent models suggesting relatively oxidized, water-rich CHO fluids as the most likely parents for lithospheric diamonds.

Published by Copernicus Publications on behalf of the European mineralogical societies DMG, SEM, SIMP & SFMC.

1 Introduction

Virtually all mineral inclusions in diamond (98 %) formed beneath cratons at depths between about 130 and 230 km (i.e. lithospheric), with the remainder forming in the asthenosphere, transition zone or lower mantle (i.e. sub-lithospheric) (e.g. Kaminsky et al., 2001; Stachel and Harris, 2008; Shirey et al., 2013; Stachel et al., 2022). Once trapped in their diamond hosts, these inclusions remain uncorrupted over geological time and represent key geological samples from otherwise inaccessible regions of our planet. Furthermore, these minerals can reveal the physical–chemical environment in which their host diamonds were formed (Bulanova et al., 2010; Stachel and Luth, 2015; Jean et al., 2016; Nimis et al., 2016; Nestola et al., 2018).

Cr-bearing spinels $(Mg, Fe^{2+})(Cr, Al, Fe^{3+})_2O_4$ (mainly magnesiochromites, hereafter mchr in the singular) are among the more common inclusions found in the peridotitic suite of lithospheric diamonds (e.g. Sobolev, 1977; Meyer, 1987; Stachel and Harris, 2008) as well as a recurrent accessory phase in ultramafic rocks. Despite their accessory nature (Cr-bearing spinels are disseminated in quantities of less than 3 % in on- and off-craton peridotite xenoliths; Pearson et al., 2003), they are important petrogenetic and oxybarometric indicators, providing information about the physical–chemical conditions under which their host rocks formed (e.g. O'Neill and Wall, 1987; Ballhaus et al., 1991; Barnes and Roeder, 2001; Miller et al., 2016). Oxygen fugacity, fO_2, is the thermodynamic variable that allows quantification of the chemical potential of oxygen in reactions where at least one element changes its oxidation state between the reagents and products. In mantle peridotites, fO_2 is estimated from the compositions of coexisting Fe-rich minerals, such as olivine, orthopyroxene, spinel and garnet. Essentially, fO_2 reflects Earth's mantle oxidation state, which can control the speciation of carbon in fluids or melts and governs the stability of carbon-bearing phases, such as diamond and carbonate minerals (e.g. Frost and McCammon, 2008; Stagno et al., 2013).

Here, we provide the first oxygen fugacity estimate for a mchr–olivine touching inclusion pair still trapped in a diamond (Oli-CHR1) from the Udachnaya kimberlite (Siberia, Russia). The diamond, previously investigated by Nestola et al. (2014) and Nimis et al. (2016, 2019), was recovered from the run-of-mine production, the vast majority of which is from kimberlite and most unlikely from any rare accompanying xenoliths. The colourless diamond is octahedral in shape with most faces showing bevelled edges. As seen in Fig. 1, mchr dominates the inclusion pair, which is situated in a peripheral position in the diamond. Thermo-/oxybarometric analysis of the inclusion pair determined the P–T–fO_2 conditions at the time of its entrapment in the host diamond, and from this result, the physical conditions under which the crystallization of Oli-CHR1 diamond occurred could be inferred, and additionally information about the redox state of this portion of the Siberian craton at the time of diamond formation could be provided. Our knowledge of the redox and thermal state of the mantle under Udachnaya largely relies on data obtained from mantle xenoliths in the kimberlite (Ionov et al., 2010; Goncharov et al., 2012; Yaxley et al., 2012; Doucet et al., 2013; Miller et al., 2016; Liu et al., 2022). These data are supposed to constrain the physical–chemical conditions of the cratonic mantle at the time of kimberlite eruption (360 ± 7 Ma; Kinny et al., 1997) but do not generally probe the redox state of the Siberian craton at an early stage of its geological history. Despite the age of our diamond being unknown, previous geochronological work on Udachnaya diamonds has suggested two major peaks of diamond formation, dated to 3.5–3.1 and ∼ 2 Ga (Richardson and Harris, 1997; Pearson et al., 1999a, b), although slightly younger ages, 1.8(5) Ga, were also obtained (Wiggers de Vries et al., 2013). Therefore, the fO_2 recorded by inclusions in Udachnaya diamonds allows the earlier redox state of the source mantle to be evaluated. By comparing fO_2 for this inclusion pair with those of xenoliths from the same depth (ca. 180 km), we will place constraints on the redox state evolution of the Siberian cratonic lithosphere from diamond formation to kimberlite eruption. The determined fO_2 for our inclusion pair also establishes a direct link to the redox conditions for diamond formation in the lithospheric mantle and will be compared with theoretical predictions based on thermodynamic modelling of CHO fluids (Luth and Stachel, 2014).

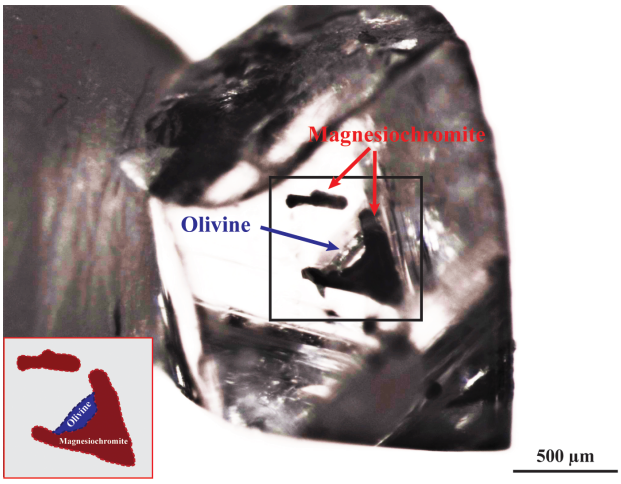

Figure 1. Close-up photograph of the Oli-CHR1 diamond shows the studied mchr–olivine inclusion pair (see also the simplified sketch of the inclusion pair, bottom left corner) and a separate elongated mchr inclusion. The larger crystal is principally cuboctahedral in shape, and both mchr inclusions are deep cherry red. The colourless olivine inclusion is attached to the larger mchr crystal, as shown. Photograph from Fabrizio Nestola's lab.

2 Experimental approach

In this work, an in situ characterization of the inclusion chemical composition was carried out by using non-destructive techniques. The sample (see Fig. 1) was analysed by (i) energy-domain synchrotron Mössbauer spectroscopy (SMS) and (ii) single-crystal X-ray diffraction (SCXRD).

2.1 Synchrotron Mössbauer spectroscopy

The SMS measurements were conducted at the nuclear resonance beamline ID18 (Rüffer and Chumakov, 1996) at the European Synchrotron Radiation Facility (ESRF), Grenoble, during operation in multibunch mode ($7/8+1$ filling). This source provides ^{57}Fe resonant radiation at 14.4 keV within a bandwidth of 15 neV which is tuneable in energy over a range of ± 0.6 µeV (i.e. ± 12 mm s^{-1}) (Potapkin et al., 2012). The X-ray beam emitted by the SMS was focused to a 16 vertical × 15 horizontal µm spot size using Kirkpatrick–Baez mirrors. Before and after sample measurement, the SMS linewidth was controlled using a $K_2Mg^{57}Fe(CN)_6$ reference single-line absorber. The velocity scale (± 5 mm s^{-1}) was calibrated relative to a 25 µm thick natural α-Fe foil. For locating the inclusion in the X-ray beam, the dedicated experimental protocol described in Nestola et al. (2016) was followed.

The acquired spectrum was fitted with a full transmission integral and a normalized Lorentzian-squared source line shape, using the software package MossA (Prescher et al., 2012). A linear function was applied to model the background.

2.2 Single-crystal X-ray diffraction

The SCXRD measurements for both minerals were conducted at the Department of Geosciences, University of Padua, with a Rigaku Oxford Diffraction SuperNova diffractometer, equipped with a Mo-target X-ray micro-source operating at 50 kV and 0.8 mA and a PILATUS 200 K Dectris hybrid pixel array detector (HPAD). The sample-to-detector distance was 68 mm, and the X-ray beam size was 0.12 mm. Data reduction was performed using the CrysAlisPro software (Rigaku Oxford Diffraction, version 40.64.67a), which allows the integration of the measured intensities and applies corrections for Lorentz-polarization effects. Unit-cell parameters along with information related to data collection and refinement details (see below) are reported in Table 1.

3 Results

3.1 Synchrotron Mössbauer spectroscopy

The resulting spectral model for the mchr (Fig. 2) shows three doublets with equal relative peak widths and areas: two are assigned to tetrahedrally coordinated Fe^{2+} and the remaining one to octahedrally coordinated Fe^{3+}. This result indicates a typically ordered distribution of Fe^{2+} and Fe^{3+} in the chromite, consistent with current crystal–chemical models (see Li et al., 2002). The spectral model for the olivine (e.g. Canil and O'Neill, 1996) includes two doublets related to the two octahedrally coordinated Fe^{2+} in the non-equivalent M1 and M2 sites, there being negligible or no Fe^{3+} content. However, only one doublet with equal relative peak widths and areas can be used to fit the olivine spectrum (e.g. Dyar et al., 2006) (Fig. 2). Also shown in Fig. 2 is the low-velocity component represented by the compound refractive lens (CRL), which is used to decrease the divergence of the beam incident to the synchrotron Mössbauer source (Potapkin et al., 2012). As it contains some iron, CRL hyperfine parameters (known from independent measurements) are accounted for in the SMS spectrum. Hyperfine parameters obtained for each specific iron structural site are reported in Table 2.

Table 1. Unit-cell parameters, data collection information and refinement details for the touching olivine and mchr inclusion in the studied diamond. Note the remarkable agreement factors of the determined crystal structures of both the olivine (R1 % = 3.2 %) and mchr (R1 % = 2.1 %) inclusions.

	Olivine	mchr
a (Å)	4.7615(2)	8.33274(6)
b (Å)	10.2003(3)	
c (Å)	5.9934(2)	
V (Å^3)	291.092(18)	578.580(12)
Space group	*Pbnm*	*Fd-3m*
Measured reflections	49 005	24 470
Unique reflections	1627	180
Reflections with Fo > 4σ(Fo)	1432	180
R1 %	3.2	2.1
GooF (goodness of fit)	1.07	1.22

3.2 Single-crystal X-ray diffraction

Structure refinement was performed using the SHELX program in the WinGX package (Farrugia, 2012; Sheldrick, 2015) in the *Fd-3m* space group for mchr and *Pbnm* space group for olivine, starting from published atomic coordinates (Nestola et al., 2011, 2019). CIF files with full refinement details are available in the Supplement. Ionic scattering curves were taken from the International Tables for X-ray Crystallography (Wilson, 1995), and anisotropic thermal parameters were refined for all atoms following Angel and Nestola (2016). The cationic distribution at the two different crystallographic sites for each inclusion was indirectly retrieved by refining the site occupancy factor of these sites (see Nestola et al., 2011, for a detailed review).

For olivine, this yielded the chemical composition $(Mg^{2+}_{0.925(2)}Fe^{2+}_{0.075(2)})_2SiO_4$, corresponding to $Fo_{92.5}$. Possi-

Table 2. Hyperfine parameters determined from the fitting of the SMS spectrum. CS ($mm\,s^{-1}$) denotes centre shift; QS ($mm\,s^{-1}$) denotes quadrupole splitting; FWHM denotes full width half maximum; Fe^{2+} [VI] denotes octahedrally coordinated Fe^{2+}; Fe^{2+} [IV] denotes tetrahedrally coordinated Fe^{2+}; Fe^{3+} [VI] denotes octahedrally coordinated Fe^{3+}; CRL denotes compound refractive lens.

Phase	Component	CS ($mm\,s^{-1}$)	QS ($mm\,s^{-1}$)	Area (%)	FWHM	$Fe^{3+}/\sum Fe$
Olivine	Fe^{2+} [VI]	1.14(1)	3.01(3)	24(6)	0.18(5)	–
mchr	Fe^{2+} [IV]	0.94(3)	0.97(10)	43(10)	0.34(9)	0.15(2)
	Fe^{2+} [IV]	0.85(4)	0.57(8)	18(13)	0.2(1)	
	Fe^{3+} [VI]	0.45(4)	0.71(6)	11(5)	0.1(1)	
CRL	–	0.15	0.41	4	0.27	

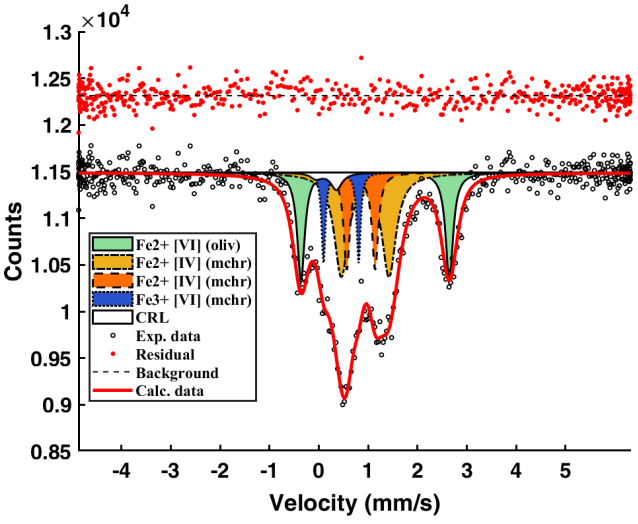

Figure 2. Energy-domain SMS spectrum of the studied mchr–olivine inclusion pair showing the contribution of both crystals. Fe^{2+} [VI] (oliv) denotes octahedrally coordinated Fe^{2+} in olivine; Fe^{2+} [IV] (mchr) denotes tetrahedrally coordinated Fe^{2+} in mchr; Fe^{3+} [VI] (mchr) denotes octahedrally coordinated Fe^{3+} in mchr; CRL denotes compound refractive lens; Exp. data denotes experimental data; Calc. data denotes calculated data. Total absorption $\sim 22\,\%$.

ble contributions from Ca, Ni, Ti, Mn, Na, Cr and K were not considered, as these elements altogether typically account for ca. 0.01 atoms per unit formula (a.p.f.u.) in mantle olivines. For example, based on 831 reviewed samples of olivine inclusions in diamonds, Stachel and Harris (2008) showed the typical content of Ni was ca. 0.007 a.p.f.u. and the total content of other minor elements amounted to a negligible average of 0.007 a.p.f.u. The chemical composition determined is well within the compositional field for olivine inclusions in diamond from Russian (Yakutian) kimberlites (Fo_{91} to Fo_{94}; Sobolev et al., 2009).

The mchr has a more complex crystal chemistry than olivine and is expected to host Mg^{2+} and Fe^{2+} in the tetrahedral site and Cr^{3+}; Al^{3+}; Fe^{3+}; and, among others, traces of Ti^{4+} in the octahedral site. In this study, the cation distribution at the tetrahedral site was retrieved by refining the site occupancy factor, but for the octahedral site, the Fe^{3+} content was calculated from the synchrotron Mössbauer $Fe^{3+}/\sum Fe$ ratio. The Ti^{4+} content was fixed to 0.004 a.p.f.u, which corresponds to the average of 815 reviewed samples of mchr inclusions in diamonds (Stachel and Harris, 2008); this value well defines an average Ti^{4+} content of mchr specifically from Yakutian diamonds (Sobolev et al., 2004). Finally, Cr^{3+} and Al^{3+} were calculated by refining the site occupancy factor. These calculations yielded the formula $(Mg^{2+}_{0.58(1)}Fe^{2+}_{0.42(1)})(Cr^{3+}_{1.75(3)}Al^{3+}_{0.17(3)}Fe^{3+}_{0.074(12)}Ti^{4+}_{0.004(7)})O_4$. If Ti^{4+} is varied within 1 standard deviation, according to Stachel and Harris (2008), the corresponding variations in Cr^{3+} and Al^{3+} contents are less than 0.005 a.p.f.u. (i.e. largely within their uncertainty). Even though minor elements other than Ti^{4+} were not considered, the calculated chemical composition is well within the compositional field of mchr from Yakutian diamonds reported in Sobolev et al. (2004). Cation distributions for the different crystallographic sites for both inclusions are reported in Table 3.

4 Discussion

4.1 Thermobarometric analysis of the inclusion pair and thermal state of the mantle

The strong dependence of fO_2 on temperature and pressure means that thermobarometric data are required to convert $Fe^{3+}/\sum Fe$ ratios and mineral chemical compositions into fO_2 values. Whilst several thermometers are available for temperature estimates of mantle samples (e.g. Brey and Kohler, 1990; Ryan et al., 1996; Taylor, 1998; Nimis and Grütter, 2010), comparatively few barometers are available for assessing pressures. This disparity is further exacerbated in mineral assemblages involving spinel, for which geobarometers are particularly limited.

In this study, the Ballhaus et al. (1991) olivine–spinel thermometer was used to calculate the last equilibration temperature of the mchr–olivine pair. Due to the slight depen-

Table 3. Cation distribution at each crystallographic site for the touching olivine and mchr inclusion in the studied diamond.

Mg and Fe cation distribution at olivine M2 and M1 sites		$Fe^{3+}/\sum Fe$ of mchr	Mg, Fe, Cr, Al and Ti cation distribution at mchr IV and VI sites		
M2 site	M1 site		IV site	VI site	
$Mg^{2+} = 0.930(3)$	$Mg^{2+} = 0.921(3)$	0.15(2)	$Mg^{2+} = 0.58(1)$	$Cr^{3+} = 1.75(3)$	$Fe^{3+} = 0.074(12)$
$Fe^{2+} = 0.070(2)$	$Fe^{2+} = 0.079(2)$		$Fe^{2+} = 0.42(1)$	$Al^{3+} = 0.17(3)$	$Ti^{4+} = 0.004(7)$

dence of this thermometer on pressure, values in the range 3.5 to 6 GPa were used as input for the thermometric calculations. Accordingly, the calculated temperatures varied between ca. 980 and 1020 °C (with an estimated error of ±50 °C). These temperatures do not necessarily indicate the conditions of diamond formation because touching inclusions may re-equilibrate during long-term mantle storage (e.g. Phillips et al., 2004; Stachel and Harris, 2008; Stachel and Luth, 2015; Viljoen et al., 2018).

With the present inclusion pair, an estimate of the entrapment pressure cannot be directly made from its chemical composition because there are no suitable geobarometers for coexisting olivine and mchr. However, assuming negligible vertical movement of the diamond in the rigid cratonic lithosphere, an approximate estimate of the entrapment pressure can be obtained by projecting thermometric estimates for the inclusion pair onto the local xenolith geotherm (Korolev et al., 2018; Nimis et al., 2020). Studies of mantle xenoliths from the Udachnaya kimberlite (Ionov et al., 2010; Goncharov et al., 2012; Yaxley et al., 2012; Doucet et al., 2013; Miller et al., 2016; Liu et al., 2022) indicate a deep lithospheric root (∼ 230 km) but show a relatively large range of geothermal gradients, spanning between the 35 and 40 mW m^{-2} model conductive geotherms of Hasterok and Chapman (2011) (see Fig. 3). To account for this geotherm range, Griffin et al. (1996) suggested that the mantle beneath Udachnaya initially experienced cold conditions as testified by ca. 35 mW m^{-2} equilibrated xenoliths (Fig. 3) but was later affected by thermal perturbations which raised the temperature of the mantle locally, especially in the deeper parts. Griffin et al. (1996) and earlier researchers (Pokhilenko et al., 1991, 1993) also noted a correlation between xenolith grain size and thermal conditions, with the fine-grained and sheared peridotite xenoliths recording higher temperatures (a feature which is commonly observed also in other cratons, e.g. Woodland and Koch, 2003), whereas the coarse-grained and megacrystalline peridotite xenoliths largely recorded lower T values falling close to a ca. 35 mW m^{-2} conductive geotherm. Liu et al. (2022) showed that heating and deformation in the deep lithospheric portion were variable, not strictly concurrent, and likely controlled by local small-scale processes. Pokhilenko et al. (1991, 1993) proposed that megacrystalline peridotite xenoliths constituted the principal host rocks of Siberian diamonds and, by extension, that the formation and storage of diamonds occurred under cold conditions consistent with a 35 mW m^{-2} conductive geotherm. Further evidence for an old, cold conductive geotherm was provided by Nestola et al. (2019), who estimated, based on elastic geobarometry and nitrogen thermometry, the P–T formation conditions for a mchr-bearing diamond from Udachnaya to be 6.5(0.2) GPa and 1125(32)–1140(33) °C. These conditions fall right on the 35 mW m^{-2} geotherm (Fig. 3), consistent with the establishment of a cold geothermal gradient over the whole Udachnaya lithosphere at the time of diamond formation. Considering the ages of diamonds at Udachnaya (3.5–3.1, ∼ 2 and ∼ 1.8 Ga; Richardson and Harris, 1997; Pearson et al., 1999a, b; Wiggers de Vries et al., 2013), these cold conditions persisted for billions of years in some portions of the Udachnaya lithosphere, particularly in the 140–190 km depth interval (Liu et al., 2022). Based on these lines of evidence, our diamond Oli-CHR1 also most likely formed and equilibrated under conditions close to a 35 mW m^{-2} geotherm. Projection of the thermometric estimates for diamond Oli-CHR1 on this geotherm (Fig. 3) yields formation conditions of $P \sim 5.7(0.4)$ GPa and $T \sim 1015(50)$ °C that are within the largely unperturbed depth interval (Liu et al., 2022). These results are fairly consistent with thermodynamic modelling in multicomponent, natural peridotitic systems (Ziberna et al., 2013), which predicts that in very depleted (highly refractory) harzburgite with bulk Cr# = 0.32 and along a 35 mW m^{-2} geotherm, spinel is stable up to 5.5 GPa and 1000 °C, where it reaches a $Cr\#_{spinel}$ of ca. 0.9, similar to that of mchr in the Oli-CHR1 diamond. Therefore, we propose that the inclusion pair did not experience any significant thermal perturbations and did not re-equilibrate after incorporation (Fig. 3); hence it records the P–T conditions of the ambient cratonic mantle at the time of its entrapment by the host diamond. Although the evidence presented above and the data reported in the literature suggest that this is the most reasonable scenario, we are aware that available age constraints suggest multi-stage diamond formation beneath Udachnaya. Consequently, if Oli-CHR1 and the diamond investigated by Nestola et al. (2019) have different ages, this implies that they may not necessarily have formed under the same geothermal gradient. An important aspect linked to different diamond ages is secular cooling of the cratonic lithosphere, which is supported both by thermal models for the formation of the cratonic roots (e.g. Michaut et al., 2009) and by the temporal change in reconstructed geotherms from

xenoliths found in Proterozoic kimberlites (Grütter, 2009). Further corroborating evidence for secular lithosphere cooling has been found in comparative studies of non-touching and touching inclusions (e.g. Phillips et al., 2004; Stachel et al., 2022). Such data show that touching inclusions generally record lower average temperatures ($\sim 100\,^{\circ}$C less) than non-touching inclusions, and this is attributed to re-equilibration in a cooling mantle until the time of eruption. However, in other cases no discrepancy exists, suggesting that diamonds formed when the lithospheric mantle had already attained a thermal regime comparable to or even colder than that existing at the time of emplacement of the host kimberlite or lamproite (Nimis, 2002). Considering all these uncertainties, we will also address a scenario in which our inclusion pair was trapped at a $\sim 100\,^{\circ}$C higher temperature, i.e. $\sim 1115\,^{\circ}$C, and eventually re-equilibrated to $\sim 1015\,^{\circ}$C during long-term mantle storage (Fig. 3). To provide any meaningful inference, such as calculating the fO_2 for the inclusion pair (see next section), the chemical compositions of olivine and mchr and specifically their Fe/(Fe + Mg) ratios have to be recalculated to $1115\,^{\circ}$C. This can be done by means of the Ballhaus et al. (1991) olivine–spinel exchange thermometer, using a trial-and-error procedure. Considering that the olivine inclusion is much smaller than the mchr inclusion, the Mg–Fe^{2+} exchange between the two inclusions would have mostly modified the olivine composition, while that of the mchr would have remained approximately constant. Accordingly, the back-calculated compositions yield χMg ~ 0.909 and χFe ~ 0.091 in olivine and χMg ~ 0.582 and $\chi Fe^{2+} \sim 0.418$ in mchr. With respect to the entrapment pressure, we will assume it to be 5.7(1.0) GPa, the larger uncertainty being related to the uncertainties in the geothermal gradient.

4.2 fO_2 analysis of the inclusion pair and oxidation state of the mantle

Oxygen fugacity in cratonic mantle has been mostly explored using xenoliths from the Kaapvaal craton in South Africa (Woodland and Koch, 2003; Creighton et al., 2009; Lazarov et al., 2009), the Slave craton in northern Canada (McCammon and Kopylova, 2004; Creighton et al., 2010) and the Siberian craton (e.g. Ashchepkov et al., 2014, 2016). These studies showed that fO_2 is close to the fayalite–magnetite–quartz (FMQ) buffer at the top of the lithospheric mantle and progressively decreases with increasing depth. These data also showed that fO_2 exhibits important lateral variations, which are commonly attributed to either melt extraction or oxidation/reduction induced by fluid or melt-driven metasomatism.

Oxybarometric data for mantle peridotite xenoliths from the Udachnaya kimberlite (Goncharov et al., 2012; Yaxley et al., 2012; Miller et al., 2016; Table S2 in the Supplement) also show this global trend with progressively lower $\Delta \log fO_2$ (FMQ) values (ΔFMQ $\simeq -1$ to $\simeq -3$, excluding outliers) with increasing depths (Fig. 4). Most of the xenoliths equilibrated at $P > 3.5$ GPa, i.e. beyond the graphite–diamond (G–D) transition, and at oxygen fugacity conditions more reduced than the enstatite–magnesite–olivine–diamond (EMOD) buffer. The EMOD buffer marks the highest oxygen fugacity at which diamonds could form and be preserved within carbonated peridotite assemblages. For calculating $\Delta \log fO_2$ (FMQ) values for our inclusion pair, the two available calibrations are from Ballhaus et al. (1991) (hereafter B91) and Nikolaev et al. (2016) (hereafter N16), both sharing the same formalism. The N16 calibration is a revision of the B91 oxybarometer based on independent experimental data and inherits much from the previous work. Here, $\Delta \log fO_2$ (FMQ) values for our inclusion pair were calculated using

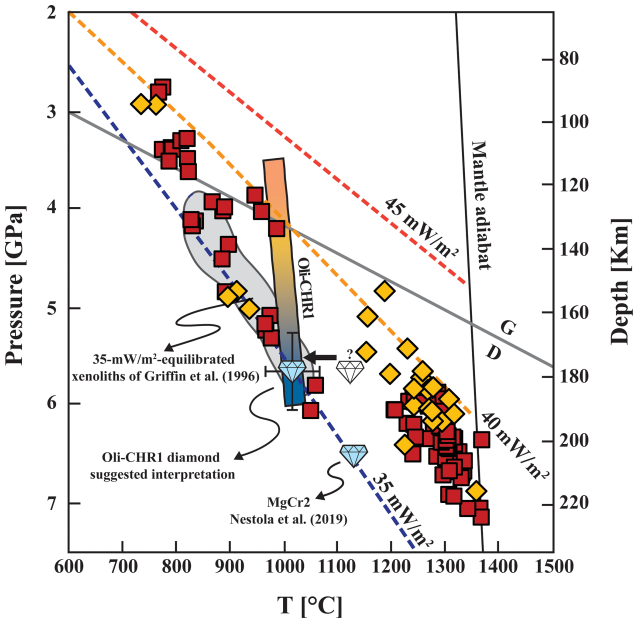

Figure 3. Pressure–temperature diagram showing the distribution of well-equilibrated mantle xenoliths from Udachnaya kimberlite (data source: Tables S1–S2). Red squares indicate the most recent P–T data from Liu et al. (2022), which include a new suite of garnet peridotite xenoliths as well as literature data (see Table S1); these data are based on a carefully selected set of well-equilibrated samples and robust thermobarometers. Yellow rhombi show the data from Goncharov et al. (2012) and Yaxley et al. (2012), for which robust P–T estimates were re-determined following Liu et al. (2022) (see Table S2). P–T conditions for the MgCr2 diamond–mchr pair from Nestola et al. (2019) and 35 mW m^{-2} equilibrated xenoliths from Griffin et al. (1996, and references therein) are also reported. The gradient bar indicates the P–T equilibration curve (see text) for the studied mchr–olivine inclusion pair; the diamond marker shows the suggested interpretation for our Oli-CHR1 diamond (see text), although entrapment at higher ($\sim 100\,^{\circ}$C) T and re-equilibration during mantle storage cannot be excluded a priori. The 35, 40 and 45 mW m^{-2} conductive geotherms for the lithospheric mantle and the 1300 °C mantle adiabat are from Hasterok and Chapman (2011); the graphite–diamond (G–D) transition is from Day (2012).

both the B91 and the N16 calibrations. Results for our preferred model, i.e. entrapment of the pair at $P \sim 5.7(0.4)$ GPa and $T \sim 1015(50)$ °C without re-equilibration after incorporation, gave $\Delta \log fO_2$ (FMQ) values of $-1.4(0.8)$ and $-1.0(0.5)$, respectively, whereas we obtained $-1.7(0.8)$ and $-1.6(0.5)$ for the scenario in which the inclusions were trapped at higher T, $\sim 1115(50)$ °C, and $P \sim 5.7(1.0)$ GPa (Fig. 4). The uncertainties in the calculated fO_2 values reported here are the nominal uncertainties for the two calibrations used. However, we are aware that our estimated chemical compositions derived from X-ray diffraction site occupancies are certainly affected by larger uncertainties than those obtained through standard electron microprobe analysis. To evaluate the uncertainties in the calculated fO_2 values which solely derive from the input parameters (i.e. statistical errors in site occupancy factors refined from SCXRD and in the $Fe^{3+}/\sum Fe$ ratio obtained from the SMS and estimated errors in thermobarometry), we applied a Gaussian error propagation function taking into account all possible error sources. In the case of entrapment of the pair at $P \sim 5.7(0.4)$ GPa and $T \sim 1015(50)$ °C, error propagation for both calibrations yielded ±0.3 log units. Of all error sources, the most critical one appears to be the uncertainty in the $Fe^{3+}/\sum Fe$ ratio of mchr, which already propagates ca. ±0.3 log units on the final fO_2 estimate for both calibrations. If the input T is changed by ±50 °C and P by ±0.4 GPa (i.e. the P–T estimate is moved within uncertainties along the 35 mW m^{-2} geotherm), the fO_2 change is only ±0.1 log units for the B91 calibration and ±0.2 log units for the N16 calibration. In the case of post-entrapment re-equilibration, an allowance for a larger pressure uncertainty (±1 GPa, due to the uncertainties in the geothermal gradient) has to be made and then taken into account with all the other possible error sources. This yielded ±0.4 log units for both calibrations. The small total uncertainty (±0.3–0.4 log units) deriving from all possible uncertainties in the input parameters is well within the nominal uncertainty in the two oxybarometer calibrations (i.e. ±0.8 log units for B91 and ±0.5 log units for N16). Additional errors probably derive from the extrapolation of both oxybarometers outside their calibration ranges (i.e. 0.3–2.7 GPa for B91 and 0.0001–2.5 GPa for N16), but these errors are difficult to estimate. Although we recognize that the extrapolation of the B91 and N16 oxybarometers at higher pressures will likely introduce further errors, the most critical issue in both cases was claimed to be the application of the corresponding formulation to some specific settings. In the case of the B91 oxybarometer, the authors advised caution when applying it to orthopyroxene-undersaturated systems or where Cr^{2+} may partially substitute in spinel, while its application to a suite of high-pressure spinels from the Archean cratonic lithosphere gave logical results (Ballhaus, 1993). Ballhaus et al. (1991) have already pointed out that the correction for orthopyroxene-undersaturated rocks rarely exceeds −0.2 log units, which falls largely within the error of the model, while

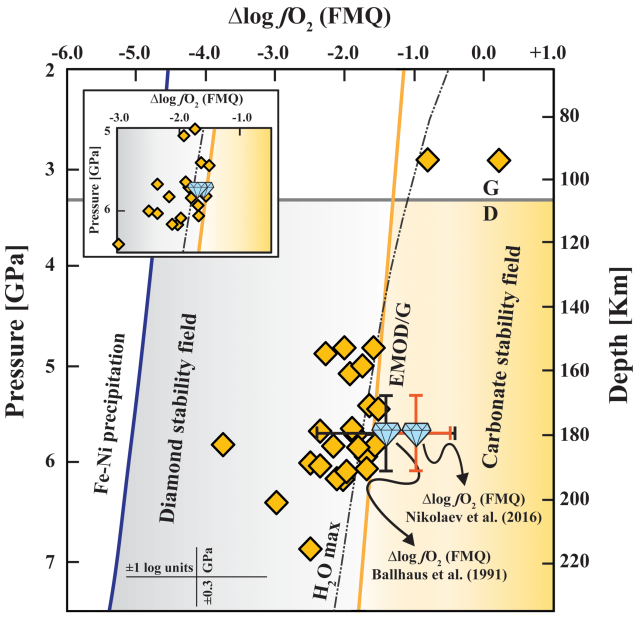

Figure 4. $\Delta \log fO_2$ (FMQ)–pressure diagram showing the distribution of well-equilibrated xenoliths from Udachnaya (yellow rhombi) (data source: Tables S2) and the calculated $\Delta \log fO_2$ (FMQ) value for the studied inclusion pair (diamond). $\Delta \log fO_2$ (FMQ) values and associated uncertainties for mantle xenoliths were calculated with the Miller et al. (2016) oxybarometer (see Table S2); typical uncertainties are shown for reference. Inset: the same data but assuming that the inclusion was trapped at ∼ 100 °C higher T and then re-equilibrated during long-term mantle storage. $\Delta \log fO_2$ (FMQ) values calculated for the inclusion pair suggest diamond formation at relatively oxidized conditions near the EMOD buffer, for both the scenarios in which the inclusion did not re-equilibrate after incorporation or was trapped at higher T. EMOD/G buffer is calculated for a 35 mW m^{-2} geotherm from the thermodynamic dataset of Holland and Powell (2011) (see Luth and Stachel, 2014, their Appendix 1); the Fe–Ni precipitation curve is from O'Neill and Wall (1987); the graphite–diamond (G–D) transition is from Day (2012) based on a 35 mW m^{-2} geotherm; the water maximum curve (labelled "H_2O max") is calculated for a 35 mW m^{-2} geotherm using the GFluid model of Zhang and Duan (2010).

significant Cr^{2+} substitution in spinel may only occur at relatively low oxygen fugacity. In the case of the N16 oxybarometer, the authors warranted caution when applying their oxybarometer to intrusive cumulus rocks, which however is not relevant in our case.

Figure 4 also shows that the EMOD line, calculated for a 35 mW m^{-2} geotherm, varies between about ΔFMQ −1.2 and −1.8 in the pressure interval 2–7 GPa. While $\Delta \log fO_2$ (FMQ) (B91) values of $-1.4(0.8)$ and $-1.7(0.8)$ are close to that of the EMOD line and fall, within error, in the diamond stability field, only the $\Delta \log fO_2$ (FMQ) (N16) of $-1.6(0.5)$ is compatible with diamond (scenario of post-entrapment re-equilibration for the inclusion), while $-1.0(0.5)$ is more ox-

idized than the EMOD line values. Nonetheless, considering all possible uncertainties, both the B91 and the N16 estimates point to relatively oxidized redox conditions comparable to, or slightly more oxidized than, those of xenoliths from the same depth (Fig. 4, Table S2), regardless of the assumed scenario. The calculated $\Delta \log f\mathrm{O_2}$ (FMQ) values for our inclusion pair are also found to be good indicators of the $f\mathrm{O_2}$ conditions of diamond formation. In fact, resetting of $f\mathrm{O_2}$ in mantle rocks may be effective and fast, given the very limited oxygen buffering capacity of depleted cratonic peridotites (Luth and Stachel, 2014; Stachel and Luth, 2015). How efficiently the $f\mathrm{O_2}$ of inclusions in diamond is reset during entrapment processes will depend on the time needed for diamond formation. Although the time required for a diamond to form in Earth's mantle is poorly known, evidence from natural diamonds and diamond growth studies suggest that this time may be geologically long. For example, monocrystalline diamonds reveal episodic growth and resorption features, indicating the presence of fluid over several millions of years (Gress et al., 2018). Experimental studies show that diamonds may grow efficiently in the presence of water and within the timescale of the experiments (e.g. Sokol and Pal'yanov, 2008; Sokol et al., 2009; Bureau et al., 2016), which were however conducted at temperatures well above those of the subcratonic lithosphere. Hence, although the time spans required for individual growth episodes and, therefore, for encapsulation of an inclusion are shorter, they are likely to be sufficiently long to allow $f\mathrm{O_2}$ resetting of the inclusion during its incorporation in the growing diamond. Based on this evidence, the inclusion pair shall record $f\mathrm{O_2}$ conditions of diamond formation, regardless of its syngenetic or protogenetic origin (cf. Nestola et al., 2014; Nimis et al., 2019). Hence, both the B91 and the N16 estimates suggest relatively oxidized conditions for diamond formation, probably falling near the upper limit for diamond stability in peridotite.

4.3 Implications for the redox state evolution and diamond formation

Archean and early Proterozoic cratons are stable regions of continental rocks with basement ages of at least 2.5 Ga (e.g. de Wit and Hart, 1993), which preserve the oldest bodies of Earth's lithosphere and contain an extensive record of its ancient history. In this context, mantle xenoliths and inclusion-bearing diamonds hosted in kimberlites are the only known direct samples of the basal lithosphere, which can deliver rare information on the nature of the lithospheric mantle and a unique perspective on the processes, conditions and evolution of the craton (Pearson and Wittig, 2014).

While the palaeo-redox state of the convecting mantle has been investigated by many researchers (e.g. Canil, 2002; Li and Lee, 2004; Aulbach and Stagno, 2016; Nicklas et al., 2019; O'Neill and Aulbach, 2022; Gao et al., 2022), suggesting a statistically significant secular increase in the mantle $f\mathrm{O_2}$ across the Archean–Proterozoic boundary, the oxygen fugacity evolution of the cratonic lithosphere has been less explored. It is well accepted that the cratonic mantle has formed by extensive melt extraction during the Archean, which left highly refractory and reducing residua because of the incompatibility of $\mathrm{Fe^{3+}}$ during melting (Frost and McCammon, 2008). This was later followed by percolation of oxidizing melts/fluids that metasomatized most of the lithospheric mantle and increased its $f\mathrm{O_2}$ over time (e.g. Foley, 2011; Foley and Fischer, 2017). However, gauging the timing of these processes is difficult because cratonic xenoliths remained open systems until the time of their entrainment in the host kimberlite. In contrast, once formed, diamonds are chemically inert containers for inclusions, which are protected from alteration/re-equilibration processes with the surrounding mantle. Therefore, the concurrent occurrence of both inclusions in diamonds, with presumably old ages, and xenoliths from the same locality allows the redox state evolution of the cratonic mantle to be unravelled.

The oxygen fugacities recorded by mantle xenoliths from Udachnaya constrain the physical–chemical conditions of the cratonic mantle at the time of xenolith entrainment in the host kimberlite (360 ± 7 Ma; Kinny et al., 1997). In contrast, the inclusion pair last equilibrated with the surrounding mantle before being encapsulated in its host diamond. Although the age of our diamond is unknown, diamonds from Udachnaya have been dated to 3.5–3.1, ~ 2 and ~ 1.8 Ga (Richardson and Harris, 1997; Pearson et al., 1999a, b; Wiggers de Vries et al., 2013), which means that the inclusion of our diamond reflects an earlier state of the cratonic lithosphere. Considering this difference in time, the similarity between $\Delta \log f\mathrm{O_2}$ (FMQ) values for mantle xenoliths from the Udachnaya kimberlite and the inclusion pair studied in this work (Fig. 4) describes a scenario in which the modern redox state of the cratonic lithosphere below Udachnaya would have likely been attained relatively early after its formation. Although the cratonic mantle has been the sink for metasomatic fluids/melts which could certainly change its redox conditions (e.g. Foley, 2011), our determination suggests that the modern redox state of this portion of the Siberian craton, once set, may have persisted for billions of years, at least at the local scale. This also agrees with evidence from multicomponent carbon isotope modelling data coupled with the prominent mode in $\delta^{13}\mathrm{C}$ values for diamonds worldwide at about -5 ± 1 ‰, which indicate that this range can be accounted for by a variation in $f\mathrm{O_2}$ of only 0.4 log units (Howell et al., 2020; Stachel et al., 2017), implying a near-constant $f\mathrm{O_2}$ through time for the mantle from which these fluids derived. Corroborating evidence was also recently observed from a comparative study of worldwide inclusions in eclogitic diamonds and eclogite xenoliths showing no systematic changes in the $f\mathrm{O_2}$ of the cratonic eclogite reservoir subsequent to diamond formation (Aulbach and Stachel, 2022), although the extrapolation of these findings to the dominant peridotite lithology should be treated with care, in

the context of its poorer oxygen buffering capacity (Luth and Stachel, 2014).

It was also recently proposed that due to the very limited oxygen buffering capacity of depleted cratonic peridotites, diamond formation in peridotites is unlikely related to rock-buffered redox reactions (Luth and Stachel, 2014; Stachel and Luth, 2015; Stachel et al., 2017). These works indicate that small amounts of O_2 (less than 200 ppm) are required to shift a peridotite from the IW (iron wüstite) to the EMOD buffer, implying that peridotites have virtually no ability to act as a source or sink for O_2 and that their oxidation state can be employed as a faithful indicator of the redox state of the last interacting metasomatic fluid. This may also apply to inclusions in diamonds, as their fO_2 is probably efficiently reset during entrapment processes (see above). Based on the poor redox buffering capacity of cratonic peridotites, Luth and Stachel (2014) have suggested that isochemical precipitation of carbon from CHO fluids under subsolidus mantle conditions may provide an efficient mode for diamond formation, especially in refractory (harzburgitic–dunitic) substrates. This would occur in response to either isobaric cooling or combined cooling and decompression as the fluid migrates upwards along a cratonic geothermal gradient. According to these models, this process can be particularly efficient if the fluid speciation is close to the water maximum, $O/(O+H)_{mol} \sim 0.33$, implying that low carbon concentrations in the fluid and high fluid / rock ratios are needed to grow diamonds. This takes place at ΔFMQ between about -1 and -2, conditions which lie very close to the EMOD buffer along a cold geotherm (Luth and Stachel, 2014) and are remarkably consistent with the relatively oxidized conditions estimated for our inclusion pair (Fig. 4). Evidence from experimental work (e.g. Sokol and Pal'yanov, 2008; Sokol et al., 2009; Bureau et al., 2016) also indicates that CHO-fluid-bearing systems at fO_2 near the water maximum promote efficient diamond growth. Nimis et al. (2020) further explored the efficiency of diamond formation processes versus depth by combining CHO-fluid modelling with various P–T paths for the ascending fluid. Their results further confirm that conditions comparable to the Udachnaya cold geotherm at 5.7 GPa at the water maximum would have good potential for diamond formation. The fO_2 estimate for our inclusion pair provides direct evidence of diamond formation under relatively oxidized conditions near the EMOD buffer, i.e. under conditions in which CHO fluids are water-rich.

We are aware that the existence of diamonds with inclusions of methane (e.g. Thomassot et al., 2007; Smit et al., 2016), carbonate or CO_2 (Schrauder and Navon, 1993; Wang et al., 1996) demonstrates that diamond formation may occur over a wide range of oxygen fugacities, in keeping with the record of deep-seated xenoliths (e.g. Yaxley et al., 2017). Although independent evidence from mantle xenoliths and carbon isotope data suggests that very reducing conditions and CH_4-rich parent media are not the norm for diamonds (Luth and Stachel, 2014; Stachel et al., 2017), more data on inclusions in diamonds similar to those provided in this work are required to determine the systematics of fO_2 conditions at which diamonds form. These data should ideally be combined with diamond age estimates to unravel the long-term redox state evolution of the cratonic lithospheric mantle.

5 Summary and conclusions

In this study, we presented the first oxygen fugacity determination of a mchr–olivine touching inclusion pair still trapped in its host diamond from the Paleozoic Udachnaya kimberlite. Thermobarometric analyses and the measured $Fe^{3+}/\sum Fe$ ratio in mchr indicate the P–T–fO_2 conditions of the inclusion pair at the time of the entrapment to be $\sim 5.7(0.4)$ GPa and $\sim 1015(50)$ °C (although entrapment at higher T and re-equilibration during subsequent mantle storage cannot be excluded) and fO_2 near the EMOD buffer. The estimated redox conditions are similar to, or slightly more oxidized than, those of xenoliths from the same depth. However, while the xenoliths last equilibrated with the surrounding mantle before their entrainment in the kimberlite at ~ 360 Ma, the inclusion pair retains the signature of a mantle as old as 3.5–3.1 Ga, ~ 2 or ~ 1.8 Ga, i.e. the known peaks of diamond formation at Udachnaya, corresponding to the time at which the mchr–olivine pair became trapped in its host diamond. Based on the similarity between xenoliths and inclusion fO_2 values, we propose that the modern redox state of this portion of the Siberian lithosphere was attained relatively early after its formation and may have persisted for billions of years, at least at the local scale, until the time of kimberlite eruption.

Moreover, the oxygen fugacity determination for our inclusion pair provides the first direct evidence for diamond formation under relatively oxidized conditions. These conditions are consistent with recent models of diamond formation suggesting water-rich CHO fluids as the most likely parents for lithospheric diamonds (Luth and Stachel, 2014).

Data availability. All data derived from this research are presented in the enclosed tables and figures and the Supplement.

Supplement. The supplement related to this article is available online at: https://doi.org/10.5194/ejm-34-549-2022-supplement.

Author contributions. LF contributed in terms of conceptualization, methodology, data evaluation and modelling, writing – original draft, and writing – review and editing; VC contributed in terms of conceptualization, methodology, and writing – review and editing; FN contributed in terms of conceptualization, methodology, writing – review and editing, and supervision; PN contributed in terms of data evaluation and modelling, writing – review and editing, and supervision; LZ contributed in terms of methodology and writing –

review and editing; LP contributed in terms of writing – review and editing; AIC contributed in terms of methodology; JWH contributed in terms of resources, writing – review and editing, and supervision; MC contributed in terms of writing – review and editing and supervision.

Competing interests. The contact author has declared that none of the authors has any competing interests.

Disclaimer. Publisher's note: Copernicus Publications remains neutral with regard to jurisdictional claims in published maps and institutional affiliations.

Acknowledgements. The European Synchrotron Radiation Facility (ESRF) is gratefully acknowledged for the provision of beam time at the ID18 nuclear resonance beamline. Luca Faccincani wishes to thank the beamline staff of ID18 and the ESRF for its traineeship programme for undergraduate students and financial support and acknowledges the Istituto Nazionale di Geofisica e Vulcanologia (INGV) for funding his PhD project (XXXV cycle) with thematic "Links between rheology, mineralogy and composition of the Earth's mantle". Luca Ziberna acknowledges the support of the Alexander von Humboldt Foundation. The authors are grateful to Sonja Aulbach and Alexander Sokol for their constructive and fruitful comments, which improved an earlier version of the manuscript. Elisabetta Rampone and Roland Stalder are acknowledged for their careful editorial handling and guidance.

Financial support. This research has been supported by an ERC Starting Grant (grant no. 307322) to Fabrizio Nestola.

Review statement. This paper was edited by Roland Stalder and reviewed by Sonja Aulbach and Alexander Sokol.

References

Angel, R. J. and Nestola, F.: A century of mineral structures: How well do we know them?, Am. Mineral., 101, 1036–1045, https://doi.org/10.2138/am-2016-5473, 2016.

Ashchepkov, I. V., Vladykin, N. N., Ntaflos, T., Kostrovitsky, S. I., Prokopiev, S. A., Downes, H., Smelov, A. P., Agashev, A. M., Logvinova, A. M., Kuligin, S. S., Tychkov, N. S., Salikhov, R. F., Stegnitsky, Y. B., Alymova, N. V., Vavilov, M. A., Minin, V. A., Babushkina, S. A., Ovchinnikov, Y. I., Karpenko, M. A., Tolstov, A. V., and Shmarov, G. P.: Layering of the lithospheric mantle beneath the Siberian Craton: Modeling using thermobarometry of mantle xenolith and xenocrysts, Tectonophysics, 634, 55–75, https://doi.org/10.1016/j.tecto.2014.07.017, 2014.

Ashchepkov, I. V., Kuligin, S. S., Vladykin, N. V., Downes, H., Vavilov, M. A., Nigmatulina, E. N., Babushkina, S. A., Tychkov, N. S., and Khmelnikova, O. S.: Comparison of mantle lithosphere beneath early Triassic kimberlite fields in Siberian craton reconstructed from deep-seated xenocrysts, Geosci. Front., 7, 639–662, https://doi.org/10.1016/j.gsf.2015.06.004, 2016.

Aulbach, S. and Stachel, T.: Evidence for oxygen-conserving diamond formation in redox-buffered subducted oceanic crust sampled as eclogite, Nat. Commun., 13, 1924, https://doi.org/10.1038/s41467-022-29567-z, 2022.

Aulbach, S. and Stagno, V.: Evidence for a reducing Archean ambient mantle and its effects on the carbon cycle, Geology, 44, 751–754, https://doi.org/10.1130/G38070.1, 2016.

Ballhaus, C.: Redox states of lithospheric and asthenospheric upper mantle, Contrib. Mineral. Petr., 114, 331–348, https://doi.org/10.1007/BF01046536, 1993.

Ballhaus, C., Berry, R. F., and Green, D. H.: High pressure experimental calibration of the olivine-orthopyroxene-spinel oxygen geobarometer: implications for the oxidation state of the upper mantle, Contrib. Mineral. Petr., 107, 27–40, https://doi.org/10.1007/BF00311183, 1991.

Barnes, S. J. and Roeder, P. L.: The Range of Spinel Compositions in Terrestrial Mafic and Ultramafic Rocks, J. Petrol., 42, 2279–2302, https://doi.org/10.1093/petrology/42.12.2279, 2001.

Brey, G. P. and Kohler, T.: Geothermobarometry in Four-phase Lherzolites II. New Thermobarometers, and Practical Assessment of Existing Thermobarometers, J. Petrol., 31, 1353–1378, https://doi.org/10.1093/petrology/31.6.1353, 1990.

Bulanova, G. P., Walter, M. J., Smith, C. B., Kohn, S. C., Armstrong, L. S., Blundy, J., and Gobbo, L.: Mineral inclusions in sublithospheric diamonds from Collier 4 kimberlite pipe, Juina, Brazil: subducted protoliths, carbonated melts and primary kimberlite magmatism, Contrib. Mineral. Petr., 160, 489–510, https://doi.org/10.1007/s00410-010-0490-6, 2010.

Bureau, H., Frost, D. J., Bolfan-Casanova, N., Leroy, C., Esteve, I., and Cordier, P.: Diamond growth in mantle fluids, Lithos, 265, 4–15, https://doi.org/10.1016/j.lithos.2016.10.004, 2016.

Canil, D.: Vanadium in peridotites, mantle redox and tectonic environments: Archean to present, Earth Planet. Sc. Lett., 195, 75–90, https://doi.org/10.1016/S0012-821X(01)00582-9, 2002.

Canil, D. and O'Neill, H. S. C.: Distribution of Ferric Iron in some Upper-Mantle Assemblages, J. Petrol., 37, 609–635, https://doi.org/10.1093/petrology/37.3.609, 1996.

Creighton, S., Stachel, T., Matveev, S., Höfer, H., McCammon, C., and Luth, R. W.: Oxidation of the Kaapvaal lithospheric mantle driven by metasomatism, Contrib. Mineral. Petr., 157, 491–504, https://doi.org/10.1007/s00410-008-0348-3, 2009.

Creighton, S., Stachel, T., Eichenberg, D., and Luth, R. W.: Oxidation state of the lithospheric mantle beneath Diavik diamond mine, central Slave craton, NWT, Canada, Contrib. Mineral. Petr., 159, 645–657, https://doi.org/10.1007/s00410-009-0446-x, 2010.

Day, H. W.: A revised diamond-graphite transition curve, Am. Mineral., 97, 52–62, https://doi.org/10.2138/am.2011.3763, 2012.

de Wit, M. J. and Hart, R. A.: Earth's earliest continental lithosphere, hydrothermal flux and crustal recycling, Lithos, 30, 309–335, https://doi.org/10.1016/0024-4937(93)90043-C, 1993.

Doucet, L. S., Ionov, D. A., and Golovin, A. V.: The origin of coarse garnet peridotites in cratonic lithosphere: new data on xenoliths from the Udachnaya kimberlite, central Siberia, Contrib. Mineral. Petr., 165, 1225–1242, https://doi.org/10.1007/s00410-013-0855-8, 2013.

Dyar, M. D., Agresti, D. G., Schaefer, M. W., Grant, C. A., and Sklute, E. C.: MÖSSBAUER SPECTROSCOPY OF EARTH AND PLANETARY MATERIALS, Annu. Rev. Earth Pl. Sc., 34, 83–125, https://doi.org/10.1146/annurev.earth.34.031405.125049, 2006.

Farrugia, L. J.: WinGX and ORTEP for Windows: an update, J. Appl. Crystallogr., 45, 849–854, https://doi.org/10.1107/S0021889812029111, 2012.

Foley, S. F.: A Reappraisal of Redox Melting in the Earth's Mantle as a Function of Tectonic Setting and Time, J. Petrol., 52, 1363–1391, https://doi.org/10.1093/petrology/egq061, 2011.

Foley, S. F. and Fischer, T. P.: An essential role for continental rifts and lithosphere in the deep carbon cycle, Nat. Geosci., 10, 897–902, https://doi.org/10.1038/s41561-017-0002-7, 2017.

Frost, D. J. and McCammon, C. A.: The Redox State of Earth's Mantle, Annu. Rev. Earth Pl. Sc., 36, 389–420, https://doi.org/10.1146/annurev.earth.36.031207.124322, 2008.

Gao, L., Liu, S., Cawood, P. A., Hu, F., Wang, J., Sun, G., and Hu, Y.: Oxidation of Archean upper mantle caused by crustal recycling, Nat. Commun., 13, 3283, https://doi.org/10.1038/s41467-022-30886-4, 2022.

Goncharov, A. G., Ionov, D. A., Doucet, L. S., and Pokhilenko, L. N.: Thermal state, oxygen fugacity and C-O-H fluid speciation in cratonic lithospheric mantle: New data on peridotite xenoliths from the Udachnaya kimberlite, Siberia, Earth Planet. Sc. Lett., 357–358, 99–110, https://doi.org/10.1016/j.epsl.2012.09.016, 2012.

Gress, M. U., Howell, D., Chinn, I. L., Speich, L., Kohn, S. C., van den Heuvel, Q., Schulten, E., Pals, A. S. M., and Davies, G. R.: Episodic diamond growth beneath the Kaapvaal Craton at Jwaneng Mine, Botswana, Mineral. Petrol., 112, 219–229, https://doi.org/10.1007/s00710-018-0582-y, 2018.

Griffin, W. L., Kaminsky, F. V., Ryan, C. G., O'Reilly, S. Y., Win, T. T., and Ilupin, I. P.: Thermal state and composition of the lithospheric mantle beneath the Daldyn kimberlite field, Yakutia, Tectonophysics, 262, 19–33, https://doi.org/10.1016/0040-1951(96)00008-X, 1996.

Grütter, H. S.: Pyroxene xenocryst geotherms: Techniques and application, Lithos, 112, 1167–1178, https://doi.org/10.1016/j.lithos.2009.03.023, 2009.

Hasterok, D. and Chapman, D. S.: Heat production and geotherms for the continental lithosphere, Earth Planet. Sc. Lett., 307, 59–70, https://doi.org/10.1016/j.epsl.2011.04.034, 2011.

Holland, T. J. B. and Powell, R.: An improved and extended internally consistent thermodynamic dataset for phases of petrological interest, involving a new equation of state for solids, J. Metamorph. Geol., 29, 333–383, https://doi.org/10.1111/j.1525-1314.2010.00923.x, 2011.

Howell, D., Stachel, T., Stern, R. A., Pearson, D. G., Nestola, F., Hardman, M. F., Harris, J. W., Jaques, A. L., Shirey, S. B., Cartigny, P., Smit, K. V., Aulbach, S., Brenker, F. E., Jacob, D. E., Thomassot, E., Walter, M. J., and Navon, O.: Deep carbon through time: Earth's diamond record and its implications for carbon cycling and fluid speciation in the mantle, Geochim. Cosmochim. Ac., 275, 99–122, https://doi.org/10.1016/j.gca.2020.02.011, 2020.

Ionov, D. A., Doucet, L. S., and Ashchepkov, I. V.: Composition of the Lithospheric Mantle in the Siberian Craton: New Constraints from Fresh Peridotites in the Udachnaya-East Kimberlite, J. Petrol., 51, 2177–2210, https://doi.org/10.1093/petrology/egq053, 2010.

Jean, M. M., Taylor, L. A., Howarth, G. H., Peslier, A. H., Fedele, L., Bodnar, R. J., Guan, Y., Doucet, L. S., Ionov, D. A., Logvinova, A. M., Golovin, A. V., and Sobolev, N. V.: Olivine inclusions in Siberian diamonds and mantle xenoliths: Contrasting water and trace-element contents, Lithos, 265, 31–41, https://doi.org/10.1016/j.lithos.2016.07.023, 2016.

Kaminsky, F., Zakharchenko, O., Davies, R., Griffin, W., Khachatryan-Blinova, G., and Shiryaev, A.: Superdeep diamonds from the Juina area, Mato Grosso State, Brazil, Contrib. Mineral. Petr., 140, 734–753, https://doi.org/10.1007/s004100000221, 2001.

Kinny, P. D., Griffin, B., Heaman, L. M., Brakhfogel, F. F., and Spetsius, Z. V.: SHRIMP U-Pb ages of perovskite from Yakutian kimberlites, Geol. I Geofiz., 38, 91–99, 1997.

Korolev, N. M., Kopylova, M., Bussweiler, Y., Pearson, D. G., Gurney, J., and Davidson, J.: The uniquely high-temperature character of Cullinan diamonds: A signature of the Bushveld mantle plume?, 304–307, 362–373, https://doi.org/10.1016/j.lithos.2018.02.011, 2018.

Lazarov, M., Woodland, A. B., and Brey, G. P.: Thermal state and redox conditions of the Kaapvaal mantle: A study of xenoliths from the Finsch mine, South Africa, 112, 913–923, https://doi.org/10.1016/j.lithos.2009.03.035, 2009.

Li, Z., Ping, J. Y., Jin, M. Z., and Liu, M. L.: Distribution of Fe^{2+} and Fe^{3+} and next-nearest neighbour effects in natural chromites: comparison between results of QSD and Lorentzian doublet analysis, Phys. Chem. Miner., 29, 485–494, https://doi.org/10.1007/s00269-002-0258-2, 2002.

Li, Z.-X. A. and Lee, C.-T. A.: The constancy of upper mantle fO_2 through time inferred from V/Sc ratios in basalts, Earth Planet. Sc. Lett., 228, 483–493, https://doi.org/10.1016/j.epsl.2004.10.006, 2004.

Liu, Z., Ionov, D. A., Nimis, P., Xu, Y., He, P., and Golovin, A. V.: Thermal and compositional anomalies in a detailed xenolith-based lithospheric mantle profile of the Siberian craton and the origin of seismic midlithosphere discontinuities, Geology, 50, 891–896, https://doi.org/10.1130/G49947.1, 2022.

Luth, R. W. and Stachel, T.: The buffering capacity of lithospheric mantle: implications for diamond formation, Contrib. Mineral. Petr., 168, 1083, https://doi.org/10.1007/s00410-014-1083-6, 2014.

McCammon, C. and Kopylova, M. G.: A redox profile of the Slave mantle and oxygen fugacity control in the cratonic mantle, Contrib. Mineral. Petr., 148, 55–68, https://doi.org/10.1007/s00410-004-0583-1, 2004.

Meyer, H. O. A.: Inclusions in diamond, in: Mantle Xenoliths, edited by: Nixon, P. H., John Wiley & Sons, Chichester, United Kingdom, 501–523, 1987.

Michaut, C., Jaupart, C., and Mareschal, J.-C.: Thermal evolution of cratonic roots, Lithos, 109, 47–60, https://doi.org/10.1016/j.lithos.2008.05.008, 2009.

Miller, W. G. R., Holland, T. J. B., and Gibson, S. A.: Garnet and Spinel Oxybarometers: New Internally Consistent Multi-equilibria Models with Applications to the Oxidation State of the Lithospheric Mantle, J. Petrol., 57, 1199–1222, https://doi.org/10.1093/petrology/egw037, 2016.

Nestola, F., Nimis, P., Ziberna, L., Longo, M., Marzoli, A., Harris, J. W., Manghnani, M. H., and Fedortchouk, Y.: First crystal-structure determination of olivine in diamond: Composition and implications for provenance in the Earth's mantle, Earth Planet. Sc. Lett., 305, 249–255, https://doi.org/10.1016/j.epsl.2011.03.007, 2011.

Nestola, F., Nimis, P., Angel, R. J., Milani, S., Bruno, M., Prencipe, M., and Harris, J. W.: Olivine with diamond-imposed morphology included in diamonds. Syngenesis or protogenesis?, Int. Geol. Rev., 56, 1658–1667, https://doi.org/10.1080/00206814.2014.956153, 2014.

Nestola, F., Cerantola, V., Milani, S., Anzolini, C., McCammon, C., Novella, D., Kupenko, I., Chumakov, A., Rüffer, R., and Harris, J. W.: Synchrotron Mössbauer Source technique for in situ measurement of iron-bearing inclusions in natural diamonds, Lithos, 265, 328–333, https://doi.org/10.1016/j.lithos.2016.06.016, 2016.

Nestola, F., Korolev, N., Kopylova, M., Rotiroti, N., Pearson, D. G., Pamato, M. G., Alvaro, M., Peruzzo, L., Gurney, J. J., Moore, A. E., and Davidson, J.: $CaSiO_3$ perovskite in diamond indicates the recycling of oceanic crust into the lower mantle, Nature, 555, 237–241, https://doi.org/10.1038/nature25972, 2018.

Nestola, F., Zaffiro, G., Mazzucchelli, M. L., Nimis, P., Andreozzi, G. B., Periotto, B., Princivalle, F., Lenaz, D., Secco, L., Pasqualetto, L., Logvinova, A. M., Sobolev, N. V., Lorenzetti, A., and Harris, J. W.: Diamond-inclusion system recording old deep lithosphere conditions at Udachnaya (Siberia), Sci. Rep.-UK, 9, 12586, https://doi.org/10.1038/s41598-019-48778-x, 2019.

Nicklas, R. W., Puchtel, I. S., Ash, R. D., Piccoli, P. M., Hanski, E., Nisbet, E. G., Waterton, P., Pearson, D. G., and Anbar, A. D.: Secular mantle oxidation across the Archean-Proterozoic boundary: Evidence from V partitioning in komatiites and picrites, Geochim. Cosmochim. Ac., 250, 49–75, https://doi.org/10.1016/j.gca.2019.01.037, 2019.

Nikolaev, G. S., Ariskin, A. A., Barmina, G. S., Nazarov, M. A., and Almeev, R. R.: Test of the Ballhaus–Berry–Green Ol–Opx–Sp oxybarometer and calibration of a new equation for estimating the redox state of melts saturated with olivine and spinel, Geochem. Int., 54, 301–320, https://doi.org/10.1134/S0016702916040078, 2016.

Nimis, P.: The pressures and temperatures of formation of diamond based on thermobarometry of chromian diopside inclusions, Can. Mineral., 40, 871–884, 2002.

Nimis, P. and Grütter, H.: Internally consistent geothermometers for garnet peridotites and pyroxenites, Contrib. Mineral. Petr., 159, 411–427, https://doi.org/10.1007/s00410-009-0455-9, 2010.

Nimis, P., Alvaro, M., Nestola, F., Angel, R. J., Marquardt, K., Rustioni, G., Harris, J. W., and Marone, F.: First evidence of hydrous silicic fluid films around solid inclusions in gem-quality diamonds, Lithos, 260, 384–389, https://doi.org/10.1016/j.lithos.2016.05.019, 2016.

Nimis, P., Angel, R. J., Alvaro, M., Nestola, F., Harris, J. W., Casati, N., and Marone, F.: Crystallographic orientations of magnesiochromite inclusions in diamonds: what do they tell us?, Contrib. Mineral. Petr., 174, 29, https://doi.org/10.1007/s00410-019-1559-5, 2019.

Nimis, P., Preston, R., Perritt, S. H., and Chinn, I. L.: Diamond's depth distribution systematics, Lithos, 376–377, 105729, https://doi.org/10.1016/j.lithos.2020.105729, 2020.

O'Neill, C. and Aulbach, S.: Destabilization of deep oxidized mantle drove the Great Oxidation Event, Sci. Adv., 8, 1–6, https://doi.org/10.1126/sciadv.abg1626, 2022.

O'Neill, H. S. C. and Wall, V. J.: The Olivine–Orthopyroxene–Spinel Oxygen Geobarometer, the Nickel Precipitation Curve, and the Oxygen Fugacity of the Earth's Upper Mantle, J. Petrol., 28, 1169–1191, https://doi.org/10.1093/petrology/28.6.1169, 1987.

Pearson, D. G. and Wittig, N.: The Formation and Evolution of Cratonic Mantle Lithosphere – Evidence from Mantle Xenoliths, in: Treatise on Geochemistry (2nd Edn.), Vol. 3, edited by: Turekian, K. K. and Holland, H. D., Elsevier, New York, 255–292, https://doi.org/10.1016/B978-0-08-095975-7.00205-9, 2014.

Pearson, D., Shirey, S., Bulanova, G., Carlson, R., and Milledge, H.: Re-Os isotope measurements of single sulfide inclusions in a Siberian diamond and its nitrogen aggregation systematics, Geochim. Cosmochim. Ac., 63, 703–711, https://doi.org/10.1016/S0016-7037(99)00042-3, 1999a.

Pearson, D. G., Shirey, S. B., Bulanova, G. P., Carlson, R. W., and Milledge, H. J.: Dating and paragenetic distinction of diamonds using the Re-Os isotope system; application to some Siberian diamonds, in: Proceedings of the 7th International Kimberlite Conference, Vol. 2, edited by: Nixon, P. H., Red Roof Design, 11–17 April 1998, Cape Town, South Africa, 637–643, 1999b.

Pearson, D. G., Canil, D., and Shirey, S. B.: Mantle Samples Included in Volcanic Rocks: Xenoliths and Diamonds, in: Treatise on Geochemistry, Vol. 2, edited by: Carlson, R. W., Elsevier, New York, 171–275, https://doi.org/10.1107/S2053273315020926, 2003.

Phillips, D., Harris, J. W., and Viljoen, K. S.: Mineral chemistry and thermobarometry of inclusions from De Beers Pool diamonds, Kimberley, South Africa, Lithos, 77, 155–179, https://doi.org/10.1016/j.lithos.2004.04.005, 2004.

Pokhilenko, N. P., Pearson, D. G., Boyd, F. R., and Sobolev, N. V.: Megacrystalline dunites and peridotites: hosts for Siberian diamonds, Carnegie I. Wash., 90, 11–18, 1991.

Pokhilenko, N. P., Sobolev, N. V, Boyd, F. R., Pearson, D. G., and Shimizu, N.: Megacrystalline pyrope peridotites in the lithosphere of the Siberian platform: mineralogy, geochemical peculiarities and the problem of their origin, Russ. Geol. Geophys., 34, 56–67, 1993.

Potapkin, V., Chumakov, A., Smirnov, G., Celse, J., Rüffer, R., McCammon, C. A., and Dubrovinsky, L.: The ^{57}Fe Synchrotron Mössbauer Source at the ESRF, J. Synchrotron. Radiat., 19, 559–569, https://doi.org/10.1107/S0909049512015579, 2012.

Prescher, C., McCammon, C. A., and Dubrovinsky, L.: MossA: a program for analyzing energy-domain Mössbauer spectra from conventional and synchrotron sources, J. Appl. Crystallogr., 45, 329–331, https://doi.org/10.1107/s0021889812004979, 2012.

Richardson, S. H. and Harris, J. W.: Antiquity of peridotitic diamonds from the Siberian craton, Earth Planet. Sc. Lett., 151, 271–277, https://doi.org/10.1016/S0012-821X(97)81853-5, 1997.

Rüffer, R. and Chumakov, A. I.: Nuclear-resonance beamline at ESRF, Hyperfine Interact., 97–98, 586–604, 1996.

Ryan, C. G., Griffin, W. L., and Pearson, N. J.: Garnet geotherms: Pressure-temperature data from Cr-pyrope garnet xenocrysts in

volcanic rocks, J. Geophys. Res.-Sol. Ea., 101, 5611–5625, https://doi.org/10.1029/95JB03207, 1996.

Schrauder, M. and Navon, O.: Solid carbon dioxide in a natural diamond, Nature, 365, 42–44, https://doi.org/10.1038/365042a0, 1993.

Sheldrick, G. M.: Crystal structure refinement with SHELXL, Acta Crystallogr. C, 71, 3–8, https://doi.org/10.1107/s2053229614024218, 2015.

Shirey, S. B., Cartigny, P., Frost, D. J., Keshav, S., Nestola, F., Nimis, P., Pearson, D. G., Sobolev, N., and Walter, M. J.: Diamonds and the Geology of Mantle Carbon, in: Carbon in Earth, Reviews in Mineralogy and Geochemistry, Vol. 75, edited by: Hazen, R. M., Jones, A. P., and Baross, J. A., Mineralogical Society of America, 355–421, https://doi.org/10.2138/rmg.2013.75.12, 2013

Smit, K. V., Shirey, S. B., Stern, R. A., Steele, A., and Wang, W.: Diamond growth from C–H–N–O recycled fluids in the lithosphere: Evidence from CH 4 micro-inclusions and δ^{13}C–δ^{15}N–N content in Marange mixed-habit diamonds, Lithos, 265, 68–81, https://doi.org/10.1016/j.lithos.2016.03.015, 2016.

Sobolev, N. V.: Deep-seated inclusions in kimberlites and the problem of the composition of the upper mantle, American Geophysical Union, Special Publications Series Vol. 11, edited by: Sobolev, N. V. and Boyd, F. R., translated by: Brown, D. A., Wiley, Washington, 279 pp., https://doi.org/10.1029/SP011, 1977.

Sobolev, N. V., Logvinova, A. M., Zedgenizov, D. A., Seryotkin, Y. V., Yefimova, E. S., Floss, C., and Taylor, L. A.: Mineral inclusions in microdiamonds and macrodiamonds from kimberlites of Yakutia: a comparative study, Lithos, 77, 225–242, https://doi.org/10.1016/j.lithos.2004.04.001, 2004.

Sobolev, N. V., Logvinova, A. M., Zedgenizov, D. A., Pokhilenko, N. P., Malygina, E. V., Kuzmin, D. V., and Sobolev, A. V.: Petrogenetic significance of minor elements in olivines from diamonds and peridotite xenoliths from kimberlites of Yakutia, Lithos, 112, 701–713, https://doi.org/10.1016/j.lithos.2009.06.038, 2009.

Sokol, A. G. and Pal'yanov, Y. N.: Diamond formation in the system MgO–SiO_2–H_2O–C at 7.5 GPa and 1,600 °C, Contrib. Mineral. Petr., 155, 33–43, https://doi.org/10.1007/s00410-007-0221-9, 2008.

Sokol, A. G., Palyanova, G. A., Palyanov, Y. N., Tomilenko, A. A., and Melenevsky, V. N.: Fluid regime and diamond formation in the reduced mantle: Experimental constraints, Geochim. Cosmochim. Ac., 73, 5820–5834, https://doi.org/10.1016/j.gca.2009.06.010, 2009.

Stachel, T. and Harris, J. W.: The origin of cratonic diamonds – Constraints from mineral inclusions, Ore Geol. Rev., 34, 5–32, https://doi.org/10.1016/j.oregeorev.2007.05.002, 2008.

Stachel, T. and Luth, R. W.: Diamond formation – Where, when and how?, Lithos, 220–223, 200–220, https://doi.org/10.1016/j.lithos.2015.01.028, 2015.

Stachel, T., Chacko, T., and Luth, R. W.: Carbon isotope fractionation during diamond growth in depleted peridotite: Counterintuitive insights from modelling water-maximum CHO fluids as multi-component systems, Earth Planet. Sc. Lett., 473, 44–51, https://doi.org/10.1016/j.epsl.2017.05.037, 2017.

Stachel, T., Aulbach, S., and Harris, J. W.: Mineral Inclusions in Lithospheric Diamonds, Rev. Mineral. Geochem., 88, 307–391, https://doi.org/10.2138/rmg.2022.88.06, 2022.

Stagno, V., Ojwang, D. O., McCammon, C. A., and Frost, D. J.: The oxidation state of the mantle and the extraction of carbon from Earth's interior, Nature, 493, 84–88, https://doi.org/10.1038/nature11679, 2013.

Taylor, W. R.: An experimental test of some geothermometer and geobaro-meter formulations for upper mantle peridotites with application to the ther-mobarometry of fertile lherzolite and garnet websterite, Neues Jb. Miner. Abh., 172, 381–408, https://doi.org/10.1127/njma/172/1998/381, 1998.

Thomassot, E., Cartigny, P., Harris, J. W., and Fanusviljoen, K.: Methane-related diamond crystallization in the Earth's mantle: Stable isotope evidences from a single diamond-bearing xenolith, Earth Planet. Sc. Lett., 257, 362–371, https://doi.org/10.1016/j.epsl.2007.02.020, 2007.

Viljoen, K. S., Perritt, S. H., and Chinn, I. L.: An unusual suite of eclogitic, websteritic and transitional websteritic-lherzolitic diamonds from the Voorspoed kimberlite in South Africa: Mineral inclusions and infrared characteristics, Lithos, 320–321, 416–434, https://doi.org/10.1016/j.lithos.2018.09.034, 2018.

Wang, A., Pasteris, J. D., Meyer, H. O. A., and Dele-Duboi, M. L.: Magnesite-bearing inclusion assemblage in natural diamond, Earth Planet. Sc. Lett., 141, 293–306, https://doi.org/10.1016/0012-821X(96)00053-2, 1996.

Wiggers de Vries, D. F., Pearson, D. G., Bulanova, G. P., Smelov, A. P., Pavlushin, A. D., and Davies, G. R.: Re–Os dating of sulphide inclusions zonally distributed in single Yakutian diamonds: Evidence for multiple episodes of Proterozoic formation and protracted timescales of diamond growth, Geochim. Cosmochim. Ac., 120, 363–394, https://doi.org/10.1016/j.gca.2013.06.035, 2013.

Wilson, A. J. C. (Ed.): International Tables for Crystallography, Vol. C, Mathematical, Physical and Chemical Tables, Kluwer Academic Publishers, Dordrecht, https://doi.org/10.1002/crat.2170280117, 1995.

Woodland, A. and Koch, M.: Variation in oxygen fugacity with depth in the upper mantle beneath the Kaapvaal craton, Southern Africa, Earth Planet. Sc. Lett., 214, 295–310, https://doi.org/10.1016/S0012-821X(03)00379-0, 2003.

Yaxley, G. M., Berry, A. J., Kamenetsky, V. S., Woodland, A. B., and Golovin, A. V.: An oxygen fugacity profile through the Siberian Craton – Fe K-edge XANES determinations of $Fe^{3+}/\sum Fe$ in garnets in peridotite xenoliths from the Udachnaya East kimberlite, Lithos, 140–141, 142–151, https://doi.org/10.1016/j.lithos.2012.01.016, 2012.

Yaxley, G. M., Berry, A. J., Rosenthal, A., Woodland, A. B., and Paterson, D.: Redox preconditioning deep cratonic lithosphere for kimberlite genesis – evidence from the central Slave Craton, Sci. Rep.-UK, 7, 30, https://doi.org/10.1038/s41598-017-00049-3, 2017.

Zhang, C. and Duan, Z.: GFluid: An Excel spreadsheet for investigating C–O–H fluid composition under high temperatures and pressures, Comput. Geosci., 36, 569–572, https://doi.org/10.1016/j.cageo.2009.05.008, 2010.

Ziberna, L., Klemme, S., and Nimis, P.: Garnet and spinel in fertile and depleted mantle: insights from thermodynamic modelling, Contrib. Mineral. Petr., 166, 411–421, https://doi.org/10.1007/s00410-013-0882-5, 2013.